

Aperture Plane Potential Control for Thermal Ion Measurements

R. C. OLSEN

Physics Department, University of Alabama in Huntsville

C. R. CHAPPELL

Space Science Laboratory

NASA Marshall Space Flight Center, Huntsville, Alabama

J. L. BURCH

Southwest Research Institute, San Antonio, Texas

Thermal plasma measurements from the Dynamics Explorer 1 spacecraft using an aperture bias in the outer plasmasphere and over the polar cap show the existence of cold plasma ($T \sim 1$ eV) which may otherwise be hidden from the particle detector by positive spacecraft potentials. Operations of the retarding ion mass spectrometer instrument with the external aperture plane biased up to -8 V with respect to the spacecraft reveal the existence of low-energy (few eV) field-aligned flows over the polar cap. Electrostatic models of the spacecraft indicate that if the spacecraft potential is more than a few volts positive, there can be a saddle point, or an electrostatic barrier, inhibiting the effectiveness of the aperture bias. Comparison of the aperture bias experiments with the electrostatic models shows that the aperture bias is successful in allowing the measurement of those field-aligned flows with kinetic energy greater than the predicted barrier height but is less effective in aiding the measurement of the isotropic background. The addition of electron measurements from the high-altitude plasma instrument allows the determination of the spacecraft potential when it is greater than +5 V. This additional information allows us to determine that the dayside polar wind (reported by Sojka et al., 1983) is supersonic, up to Mach 5.

1. INTRODUCTION

1.1. History

Plasma measurements in the magnetosphere have always depended upon an accurate knowledge of the satellite potential, particularly when the magnitude of the satellite potential is comparable to the energy of the measured particles. Measurement of the attracted species generally only requires care in the data analysis, but measurement of the repelled species requires the assumption that the portion of the distribution which is measured is characteristic of that at lower energies. Recent measurements on geosynchronous satellites in eclipse show that this is not always a valid assumption and that there can be plasma distributions at low energies which cannot be inferred from the higher-energy tail [Olsen, 1982].

Because of this problem, some form of potential control is required, particularly for ion measurements in regions where the satellite potential is positive, i.e., everywhere outside the plasmasphere. An example of this is the S-302 experiment on GEOS 1 and GEOS 2, the suprathermal plasma analyzers. These were electrostatic analyzers mounted on 1.8-m booms, with a range of bias voltages from +28 to -28 V. The 0.5- to 500-eV energy range was designed to cover the thermal and suprathermal ion and electron population of the outer plasmasphere and plasma sheet. The biasing technique was successful, as long as the bias voltage exceeded the spacecraft potential [Decreau et al., 1978; Johnson and Wrenn, 1983; Olsen et al., 1983].

Copyright 1986 by the American Geophysical Union.
Paper number 4A8466. 0148-0227/86/004A-8466\$05.00

For the retarding ion mass spectrometer (RIMS) on Dynamics Explorer (DE 1), potential control was in the form of an external aperture plane around the instrument which could be biased with respect to the satellite. This is not far removed from the original OGO 1 and 3 electron and ion trap design, where the voltages could be applied to the external grid, or aperture plane [Whipple and Parker, 1969a,b; Parker and Whipple, 1970; Whipple et al., 1974].

Similar capabilities were incorporated on the mass spectrometers on OGO 1, 2, 3, 4, and 6. The OGO 1 spectrometer, for example, had a guard ring which could be set at 0, -5, -10, or -15 V. Much of the OGO 1 data was taken at -15 V [Taylor et al., 1965]. The early OGO experiences differed from those on later spacecraft because the positive solar arrays and exposed solar array tabs resulted in a negative satellite potential (-15 V at low altitudes up to 0 V at high altitudes). Because of these spacecraft potentials, a negative bias on the ion detectors was not as useful as might have been anticipated. Subsequent use of a biased guard ring on the Pioneer Venus mass spectrometer has been infrequent, due to an apparent lack of need for it in the Venus environment (H. A. Taylor, private communication, 1984).

The analysis problem introduced by nonuniform voltages such as those introduced by an aperture bias is that an electrostatic barrier may be established which prevents ions from reaching the aperture, even if it were energetically possible for them to do so in the absence of a barrier. In particular, if the bias voltage is swept as on the OGO ion traps, the analysis problem is made doubly complicated by the variation in barrier height. The combinations of potentials on DE 1 differ from those experienced on the OGO satellites, but the analysis problem is similar. The purpose of this paper is to illustrate the effect of an external aperture plane on low-energy ion

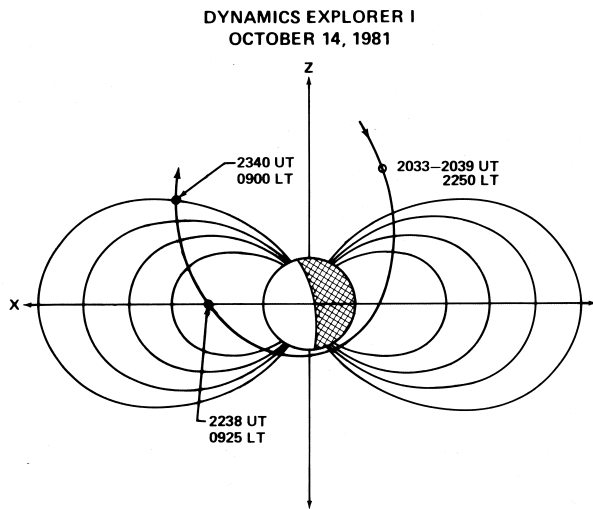


Fig. 1. Orbit plot for DE 1, October 14, 1981 (day 287). The orbit is plotted in SM coordinates, rotated to the local time of each point, i.e. rotated into an L, λ_m plane.

measurements. An electrostatic model of the aperture bias process is presented and compared to data taken in the plasmasphere and polar cap.

1.2 Spacecraft and Instruments

The DE 1 satellite was launched into a polar orbit on August 3, 1981, with a perigee of 675 km altitude and an apogee of 4.65 RE. The 7.5-hour orbit began with apogee over the north pole, with apogee moving toward the equator (in the midnight sector) in the spring of 1982. The spacecraft spins in a reverse cartwheel fashion, at 10 rpm with its spin axis perpendicular to the orbit plane.

The retarding ion mass spectrometer (RIMS) is composed of three sensor assemblies. The radial sensor head views perpendicularly to the spin axis and provides pitch angle distributions, while sensors on the ends of the space-craft view parallel to the spin axis to complete the phase space coverage. The radial sensor head has an angular resolution of $\pm 10^\circ$ in the spin plane and $\pm 55^\circ$ perpendicular to the spin plane. The end heads, or Z heads, have roughly conical apertures with 55° half angles. The instrument covers the 1-32 AMU mass range with two channels. The low channel covers the 1-8 AMU range, the high channel 4-32 AMU. In this paper, we will show only H⁺ and He⁺ data using the low (1 AMU) and high mass (4 AMU) channels in parallel. A retarding potential analyzer (RPA) precedes the mass analysis, with a voltage sweep from 0 to 50 V. In addition to the RPA, there is an external aperture plane which is normally grounded to the spacecraft body but can be biased with respect to the spacecraft to values of -2, -4, and -8 V. The diameter of the aperture plane was 20 cm, substantially smaller than the spacecraft dimensions of 1 m in height and 1.4 m in diameter. The retarding voltages are referenced to the aperture plane, so that to the RIMS detector the effect of the bias should be the same as a change in spacecraft potential, aside from the effects of local fields [Chappell et al., 1981].

Magnetic field data are obtained from the DE 1 Goddard Space Flight Center magnetometer [Farthing et al., 1981]. These data provide the pitch angle information needed to interpret the particle angular distributions.

The high-altitude plasma instrument (HAPI) consists of five sets of electrostatic analyzers arranged to cover most of velocity space in one spin period, at energies from 5 eV to 32 keV. Ions and electrons are measured with 32% energy resolution, $2.5^\circ \times 10^\circ$ angular resolution, with a sample rate of 64 s^{-1} . The geometric factor is $3.0 \times 10^{-4} \text{ sr cm}^2$ [Burch et al., 1981].

2. OBSERVATIONS

The first orbit using aperture bias data was on October 14, 1981, illustrated in Figure 1, a projection of the orbit plane in solar-magnetic coordinates. All of the data to be shown below are from this orbit. The first example of aperture bias data is from the plasmasphere, in order to illustrate the effect of the bias in an isotropic plasma, with a spacecraft potential less than 0.5 V. Next, measurements of field-aligned ions on the nightside illustrate the results of aperture bias at spacecraft potentials of a few volts. Finally, field-aligned ion measurements from the dayside, at spacecraft potentials of 8 to 10 V, show evidence of a barrier effect, and perhaps variations in the spacecraft potential caused by the bias.

2.1 Observations in the Plasmasphere

The first data to be shown come deep in the plasma-sphere, at 2 RE, near the magnetic equator (see Figure 1). The ambient plasma density is about 5000 cm^{-3} , and the spacecraft potential is a few tenths of a volt negative. In this region, there should not be any major effects due to local fields, since the Debye length is less than 10 cm and thus less than the scale size of the aperture plane. The hydrogen data illustrate subsonic flow measurements, the helium data supersonic flow. Figures 2a and 2b show the retarding potential analyzer (RPA) voltage sweeps. Data are taken in the ram direction and analyzed by using the thin sheath approximation developed by Comfort et al. [1982, 1985]. This analysis technique is based on the general formalism developed by Whipple et al. [1974]. Comfort et al. calculated the integrated instrument response for a ram plasma for the thin sheath case, obtaining an analytic form. The thin sheath case is found to be close to the solution for an arbitrary sheath, so long as the satellite potential is not large [Comfort et al., 1985]. The RPA curves in Figures 2a and 2b shift in energy, but otherwise, there are no apparent effects due to local fields, as expected in this potential regime. The variation in flux with the angle of attack (spin phase) depends upon the satellite potential. The primary effect is a broadening of the spin curve, as illustrated in Figures 2c and 2d, for hydrogen and helium, respectively. In Figure 2c, the hydrogen data are plotted versus the cosine of the ram angle. The fits to the data are based on numerical simulations of the RIMS response to flowing plasmas [Singh and Baugher, 1981; Comfort et al., 1985]. Analytical fits to the numerical simulations are used in the fitting process. For an integral flux, 28° detector, the log of the flux would be expected to show a linear dependence on cosine theta, as would the log of the distribution function for a differential detector

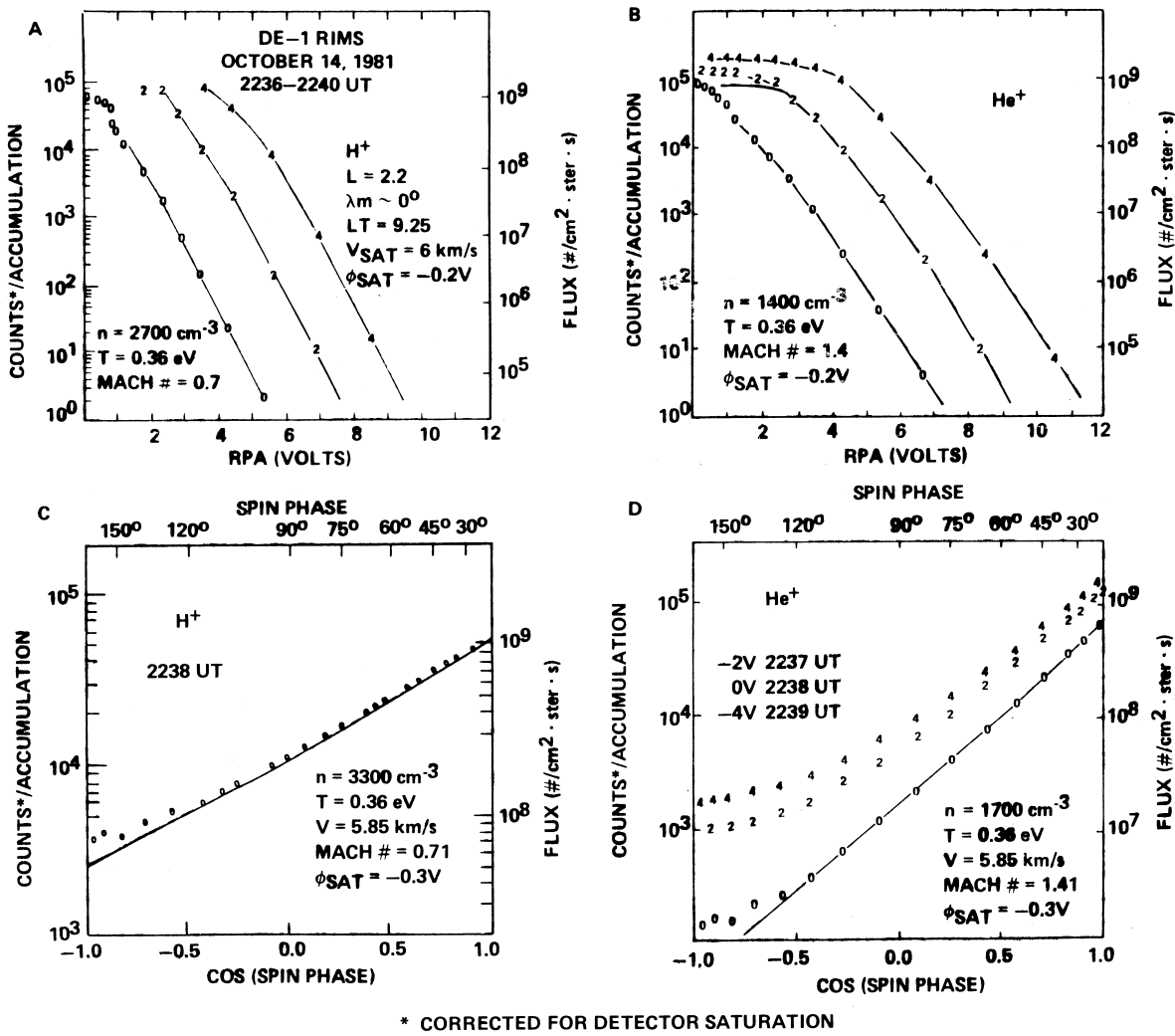


Fig. 2. Isotropic plasma measurements at low altitudes made with the radial detector. (a) Hydrogen RPA curves take in the ram direction ($\pm 10^\circ$) at 0, -2, and -4 V aperture bias. (b) Helium RPA curves taken in the ram direction. (c) hydrogen spin curve, 0 V aperture bias, RPA voltages 0.0 to 0.5 V. (d) Helium spin curves, 0, -2, -4 V aperture bias, RPA voltages 0.0 to 0.5 V.

such as an electrostatic analyzer [Wren et al., 1984]. The limited aperture, integral energy detector will not strictly depend upon the cosine of the ram angle, but as illustrated in Figure 2c, the deviation from a straight line is minimal until entering the wake region (spin phase greater than 90°). Since it is difficult to model the wake data anyway, this is not a serious restriction. Just as with energy distributions, variations in temperature (Mach number) cause the slope to vary. Variations in spacecraft potential cause relatively smaller variations in slope. Detector saturation effects are fairly severe for the hydrogen data at this time, so we concentrate on the helium data to illustrate the variations in the spin curves with aperture potential.

Figure 2d shows the helium spin curves for aperture biases of 0, -2, and -4 V. The peaks of the -2 V and much of the -4 V data have been corrected for detector saturation effects, beginning near the 80,000 count (6 MHz) level. It can be seen

that the peak flux increases, as might be expected, but more importantly, the tails of the spin curves (the wake data) increase by much larger percentages. This effect is also illustrated by eclipse measurements reported by Olsen et al. [1985]. This characteristic of the spin curves is important for the analysis of the data taken at higher altitudes and the inference of barrier effects which follows.

2.2. Observations in the Polar Cap

Continuing on the same day, we next present data taken at a higher spacecraft potential, between +2 and +4 V. The upper limit on the potential is determined from the electrostatic analyzer data (HAPI). No spacecraft-generated photo-electrons are observed by HAPI, indicating that the potential is below 4 V (the low-energy limit of the lowest channel). In the nightside polar cap, the aperture bias

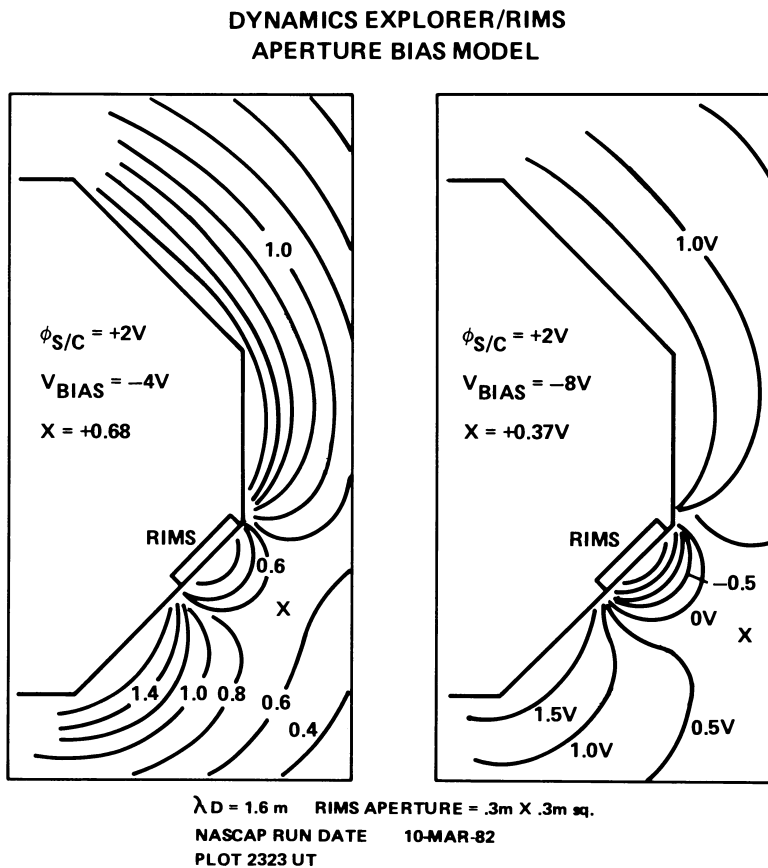


Fig. 3. Isopotential contours for a model of the DE 1 satellite with biased RIMS radial aperture. The saddle points are marked with crosses. Note that the contours plotted do not extend all the way to the aperture potentials (-2 and -6 V), due to limits in the plot resolution.

operations revealed a high-velocity (10-20 km/s) field-aligned hydrogen flow, in spite of the positive spacecraft potential. Plate 1a shows the hydrogen data from the radial detector in a spin-energy time spectrogram. The top panel shows the RPA sweeps for the data taken along the magnetic field line, the bottom curve the angular distribution of the data taken at energies between 0.0 and 0.5 eV. The aperture bias is sequenced in a regular pattern throughout this period, 0 V, -2 V, 0 V, -4 V, 0 V, -8 V, and so on. The highest fluxes are seen at -8 V, as expected. From 2034 and 2040 UT, the top panel shows green at energies less than 1 eV, showing 5-10 counts per accumulation in the field-aligned direction even at 0 V bias. In addition to the field-aligned flow, a cold rammed plasma appears at -4 and -8 V bias, as seen in the lower panel. The detector view direction is plotted on the vertical axis of the lower panel, with views in the direction of the spacecraft motion (RAM direction) at 0°. The relationship to the magnetic field directions is indicated by the solid and dashed white lines running horizontally across the plot. The solid line is for 180° pitch angle (flow from the north geographic pole), while the dashed line is for 0° pitch angle.

These data have been interpreted by Nagai et al. [1984] as the first high-altitude measurements of the supersonic polar wind. The lower half of Plate 1 shows the He+ data for the same time segment. A field-aligned helium population is also found, as discussed (but not shown) by Nagai et al. The helium flux is lower than the hydrogen flux by an order of magnitude but is otherwise similar to the field-aligned hydrogen flow.

The plasma wave instrument provides a different perspective on this time period. Wave data can often be used to obtain a plasma density, using features associated with the plasma frequency. In this case, the wave data suggest that this is an unusual day and that there may be an isotropic background which is difficult to measure, even with the aperture bias. The plasma wave data for this period have been analyzed in concert with the other DE 1 experiments by Gallagher et al. [1986]. They find that there may be a background hydrogen population (non-field-aligned) with a density near 10 cm⁻³. The question then is, do the aperture bias operations reveal such a cold plasma? RPA curves taken along the ram direction at -4 and -8 V bias (shown below) show extremely low fluxes (10 counts or

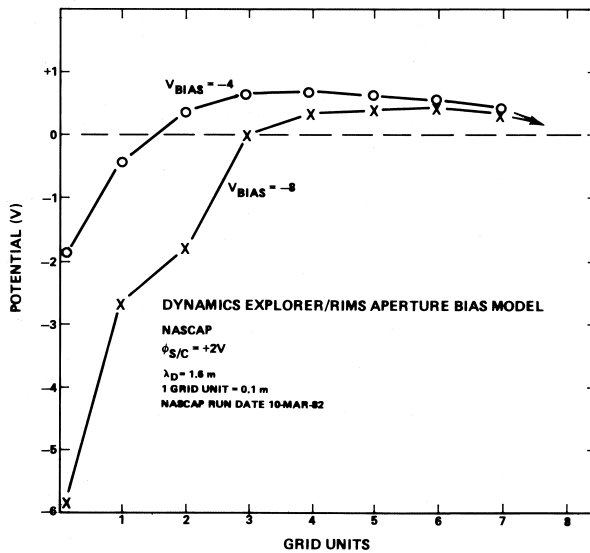


Fig. 4. Potential versus distance for the NASCAP DE 1/RIMS modeL The barrier height is the 0.5-1.0 V maximum three to six grid units from the aperture.

less per accumulation). RPA analysis without barrier effects included produced densities of 1 cm⁻³ or less. In order to further interpret these measurements, it is necessary to examine the potential distribution around the satellite resulting from the aperture bias operation.

3. MODELS

Interpretation of the plasma data requires a model for the fields around the satellite similar to that constructed by Whipple and Parker [1969a,b] for the planar geometry of OGO 1. Two models have been developed for this purpose and have been compared to the data. These comparisons show qualitative agreement between the data and models. The first model is the NASA Charging Analyzer Program (NASCAP), a three-dimensional numerical code designed to work on a 16 x 16 x 33 grid, solving Laplace's equation for a given potential distribution and a specified geometry. Space charge can safely be excluded for the 1-100 cm⁻³ density regime to be studied. The addition of Debye shielding will only lower the barrier, so we are effectively solving for the worst case. This code is normally used to model spacecraft charging dynamics, solving for the currents to and from the spacecraft, and iteratively adjusting the spacecraft potentials and cur-rents. In this case, only the potential solving portion of the code was utilized. This code was previously used successfully to model the differential charging effects observed on ATS 6 [Olsen et al., 1981]. A short cylinder was used to simulate the satellite, and a three cell by three cell surface element was used to simulate the aperture plane. The code resolution is essentially one cell.

The results for two sets of potentials are shown in Figure 3, which displays isopotential contours in a cut perpendicular to the spacecraft axis through the center of the detector. A saddle point is formed in front of the aperture, with a magnitude below 1 V. The potential distribution along a nominal particle trajectory radially away from (or toward) the detector is shown

in Figure 4. The potential maximum four grid units (0.4 m) away from the detector is a barrier to low-energy ions.

A complete set of spacecraft and aperture potentials was run with this model, with results shown in Figure 5, a plot of the barrier height versus spacecraft potential for the different aperture biases. The NASCAP predictions are shown in combination with the results from an analytic model to be described next.

The large size of the NASCAP code makes it awkward to use, and a faster, more adaptable code is needed to study the effects of aperture bias and angular effects. Also, by compromising on the geometry of the model, higher resolution is possible. Again, space charge is not included, and we solve Laplace's equation. To accomplish this, the spacecraft was modeled as a sphere, with the aperture modeled as a cap of 5°-20° half angle. Setting the sphere at spacecraft potential and biasing the cap to the aperture potential, it was possible to expand the spherical potential distribution using Legendre polynomials, in a multipole fit. The potential distribution away from the sphere can then be accurately determined with this spherical expansion, and these terms are easily evaluated.

The results from this model are illustrated in Figure 6, a plot of the potential distribution for a cap of 10° half angle. Again a barrier results. The barrier height obtained in this way is also plotted in the smooth curves in Figure 5. The two sets of plots agree in the monotonic rise in barrier height with spacecraft potential, and the drop with increasing aperture bias. The magnitudes are in rough agreement. Closer agreement could be obtained with a different solid angle for the cap, but it is felt that 10° accurately matches the ratio of areas on the actual spacecraft. The difference seen in this plot is probably largely due to the difference between cylindrical and spherical geometry.

The effects such bathers should have on RIMS data are illustrated in Figure 7. The barrier effect is incorporated into the thin sheath model by assuming an average barrier across the aperture which acts on the normal incident energy of the ions. This is done by changing the low-energy

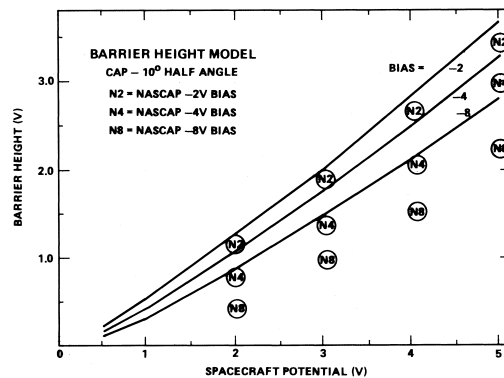


Fig. 5. Summary of the NASCAP barrier height calculations for -2, -4 and -8 V biases for 1-5 V spacecraft potentials. NASCAP model values are circled. The lines are the result of the multipole sphere model

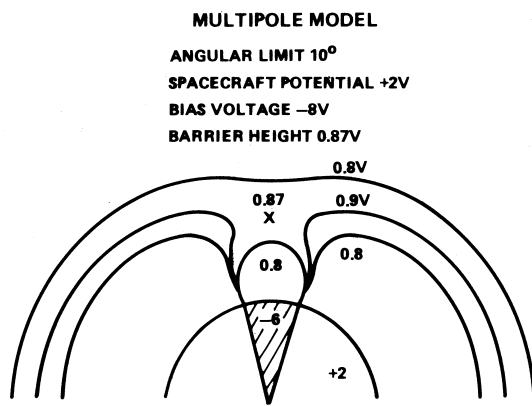


Fig. 6. Equipotential contours for a sphere at +2 V with a cap biased -8 V with respect to the sphere (-6 V). A saddle point is formed at +0.87 V.

cutoff (in the normal direction) to be the barrier height (VBARR), when the sum of the RPA voltage and satellite potential is less than the barrier height ($\phi_{RPA} + \phi_{SAT}$) $S/C < VBARR$). The first-order correction should be sufficient, given the limitations of the data. The left side of Figure 7 shows the effects of a 1-V barrier on the measurement of a cold, isotropic plasma. The data will appear to exhibit the effects of a -2 V spacecraft potential, though the potential difference between the aperture and ambient plasma is only 1 V. The right-hand side of Figure 7 shows how a high-velocity flow can overcome barrier effects, in anticipation of the polar wind measurements to be shown.

3.1. Comparison of Data With Models

3.1.1. Polar cap observations. The next step in the process is to compare these models with particle data taken at high altitudes. The field-aligned flows and the isotropic background illustrated in Plate 1 are reasonably stable from 2033 to 2045 UT. The spacecraft potential is apparently

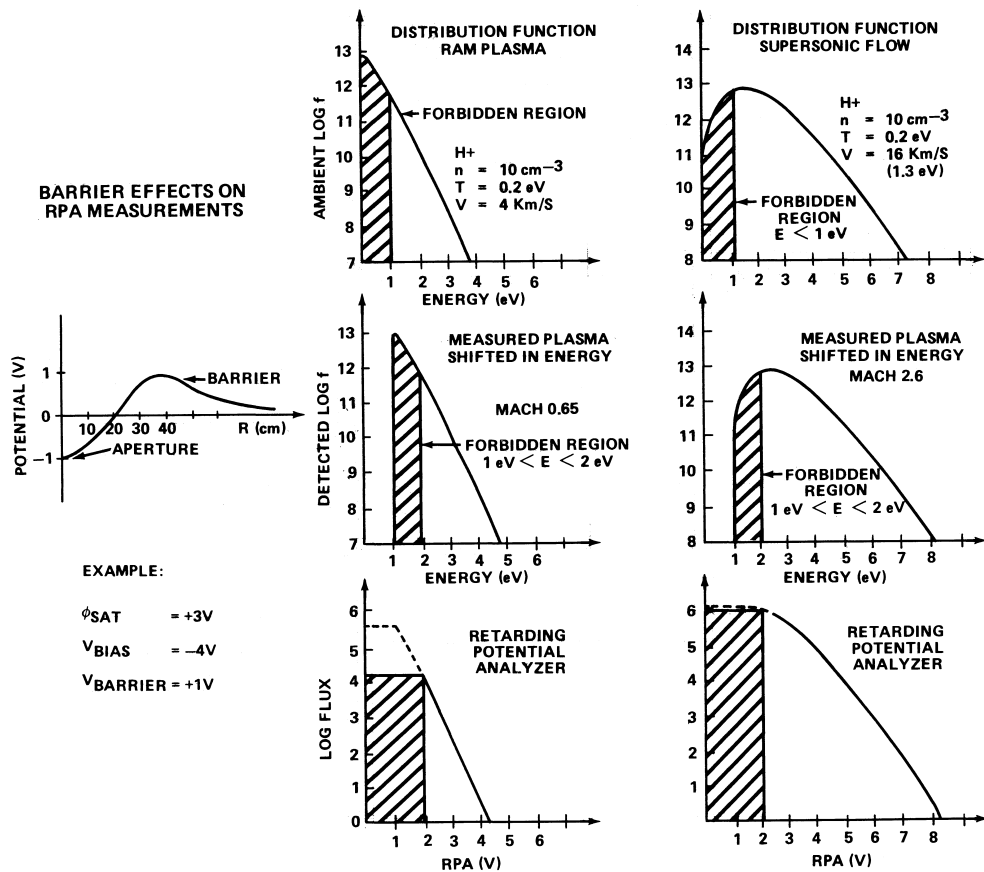


Fig. 7. Barrier effects on RPA measurements are illustrated for a ram plasma, where the flow energy is less than the barrier height, and a supersonic flow, where the flow energy is greater than the barrier height. The top figures show the ambient plasma distribution, with the forbidden region shaded. The distribution function has shifted upward in energy when it reaches the negative aperture, as shown in the middle panels. The RPA responses to such distributions are shown in the bottom panels.

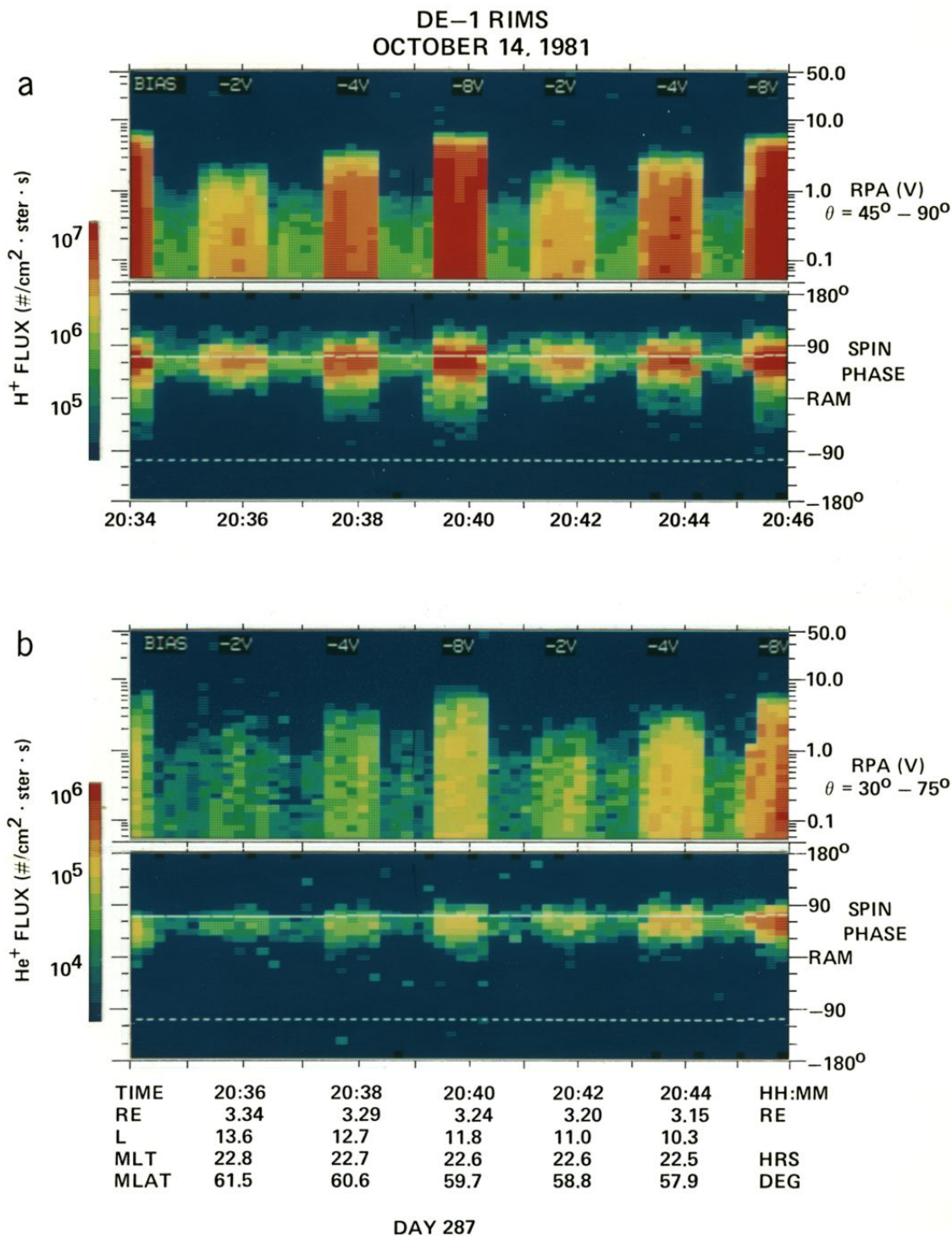


Plate 1. (a) RPA time (top panel) and spin time (bottom panel) spectrograms for the nightside polar cap hydrogen measurements. The aperture bias goes through two cycles in the 12-min period shown here, -8 V, 0 V, -2 V, 0 V, -4 V, 0 V, -8 V, etc. The RPA panel is restricted to data taken in the field-aligned direction ($0 = 45^\circ - 90^\circ$). The spin panel is limited to RPA voltages from 0.0 to 0.5 V. The solid white line between $0 = 60^\circ$ and 90° is the 180° pitch angle locus; the dashed white line between $0 = -90^\circ$ and -120° is the 0° pitch angle line. (b) As in Plate 1a, but for helium. The RPA panel is limited to $0 = 30^\circ - 75^\circ$.

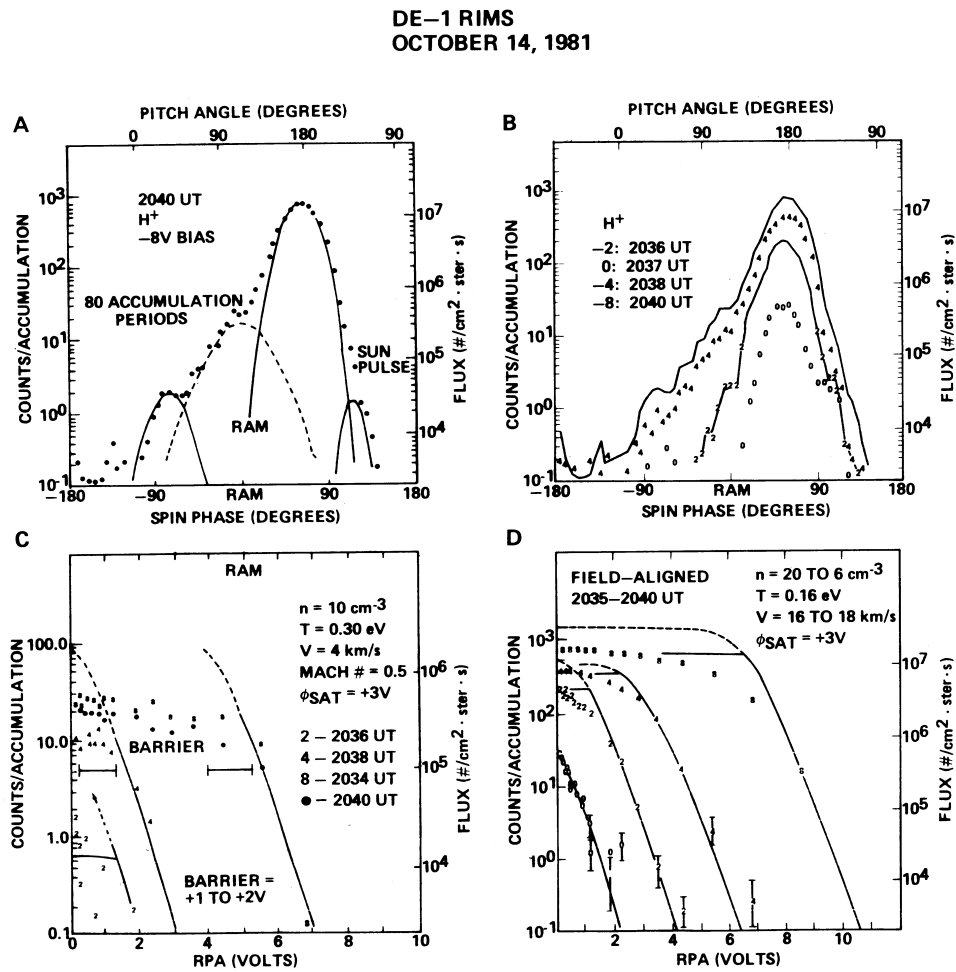


Fig. 8. Spin curves and RPA curves for the time period shown in Plate 1. (a) Spin curves for -8 V bias, 0.0-0.5 V RPA. The peak near 90° spin phase can be fitted with a flowing Maxwellian: $n = 2 \text{ cm}^{-3}$, $T = 0.2 \text{ eV}$, $V = 20 \text{ km/s}$, $\phi = 0 \text{ V}$. The downward flow near -90° spin phase can be fitted with the same Maxwellian, but $n = 0.02 \text{ cm}^{-3}$. The isotropic background dominates the central portion of the curve. (b) the -8 V bias data from Figure 8a, with 0, -2, and -4 V bias data. The upward flow persists even at 0 v bias, which can be fitted with a flowing Maxwellian with $n = 2 \text{ cm}^{-3}$, $T = 0.2 \text{ eV}$, $V = 20 \text{ km/s}$, $\phi = +3 \text{ V}$. (c) RPA data for the ram plasma ($0 = -20^\circ$ to 0°). The dashed line indicates the portion of the fit truncated by the barrier. This corresponds to the forbidden region shown in Figure 7. (d) RPA data for the upward field-aligned flow ($0 = 55^\circ$ - 65°), are fitted with flowing Maxwellians.

+3 to +4 V, as deduced below, which suggests barrier potentials of 1-2 V. These data should therefore be useful for determining the effects of local fields on observations.

Figure 8c shows data taken in the "ram" direction, i.e., the flux perpendicular to the magnetic field line, the isotropic background. The ram energy for hydrogen is negligible here (less than 0.1 eV), so the knees in the RPA curves occur at either the spacecraft potential or the energy $+0.5$

difference between the aperture plane and the energy of the saddle point (barrier). The "knee" for the -8 V bias data occurs between 4 and 5 V; the "knee" for the -4 V bias data occurs at about 1 V. These data would be consistent with a 3-V spacecraft potential or a spacecraft potential of +4 V and a barrier of slightly over 1 V. The latter situation is indicated by the low densities (1 cm⁻³) resulting from attempts to model the data without barrier effects. Also,

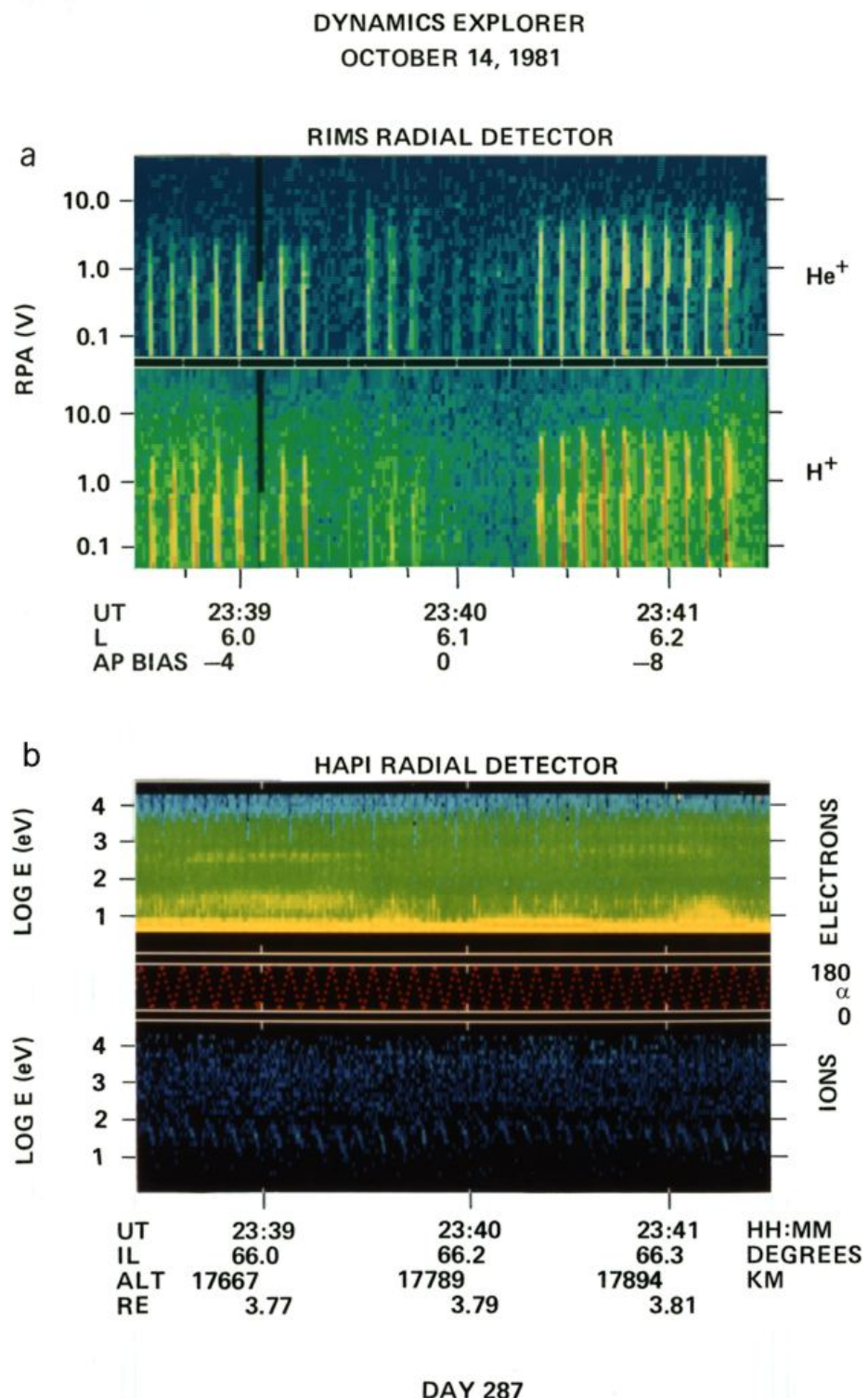


Plate 2. (a) RIMS spectrogram for a 3-min period for the radial detector. The 6-s spin period produces the modulation of hydrogen (lower panel) and helium (upper panel) fluxes. The aperture bias is cycled at 1-min intervals, here from -4 V to 0 V to -8 V. (b) HAPI spectrogram for the same period as in Plate 2a. Electron fluxes in the top panel show high fluxes at low energies, nominally locally generated photoelectrons trapped by a +10 V satellite potential.

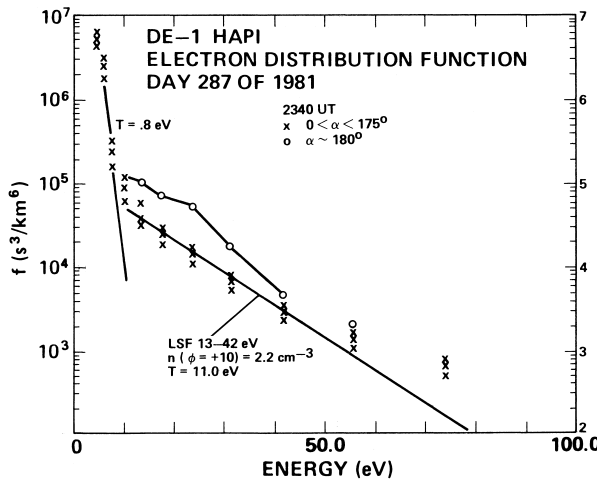


Fig. 9. Electron distribution function from HAPI. The locally generated photoelectrons show a 1-eV spectrum up to 10 V, followed by a warm (11 eV) ambient plasma distribution. Ionospheric photoelectrons are found at 180° pitch angle. These latter data were excluded from the least squares fit (LSF) to the ambient distribution.

there should be a substantially larger difference between the saturation levels of the -4 V and -8 V bias data, as indicated by the dashed lines extending up from the fits to the data. The nature of the problem is illustrated by Figure 7, which shows how the energy of the distribution function varies along the particle trajectories which reach the instrument. Ambient ions with energies less than 1 eV cannot reach the satellite. Those particles which do over-come the barrier then fall down the potential hill into the detector, resulting in integral flux measurements which are flat out to the energy corresponding to the difference in potential between the detector aperture and the barrier.

Figures 8a and 8b show the spin curves for the hydrogen data taken at RPA voltages between 0 and 1 V. The increase in flux with increasingly negative aperture bias voltages is obvious. The field-aligned flux is visible at 0 V bias,

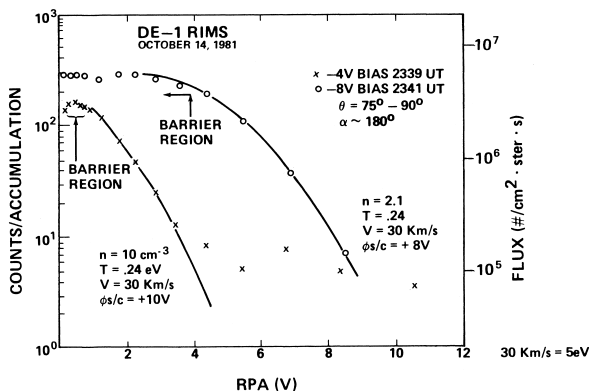


Fig. 10. RPA curves for the field-aligned hydrogen fluxes illustrated in Plate 2a.

TABLE 1. Field-Aligned Hydrogen Parameters, Day 287 of 1981, 2338–2339 UT, $V_{s/c} = 3.39 \text{ km/s}$

n, cm^{-3}	T, eV	V, km/s	E, eV	Mach Number	$\phi_{s/c}, \text{V}$
600	0.59	10	0.52	0.95	+8
130	0.50	15	1.2	1.54	+8
28	0.40	20	2.1	2.30	+8
8	0.28	25	3.3	3.43	+8
(4)	0.24	25	3.3	3.71	(+8)
2	0.15	30	4.7	5.63	+8
(0.5)	0.12	30	4.7	6.1	(+8)
800	0.55	15	1.2	1.47	+10
200	0.45	20	2.1	2.17	+10
42	0.35	25	3.3	3.07	+10
10	0.24	30	4.7	4.45	+10
(4.5)	0.20	30	4.7	4.87	(+10)
2.1	0.15	35	6.4	6.56	+10
(0.45)	0.11	35	6.4	7.66	(+10)

The RPA analysis results listed here were obtained with both the thin sheath approximation [Comfort et al., 1984] and the neutral planar approximation [Sojka et al., 1983] to facilitate comparison with the previous analysis by Sojka et al. The neutral planar model results are listed in parentheses. The energy, E, in the fourth column is the flow energy. A spacecraft potential of +8 to +10 V implies an ambient electron density of 0.1–10.0 cm⁻³,

with a ram component becoming visible at -4 and -8 V bias. At -8 V bias, there is a hint of a small flux of downward flowing ions (0° pitch angle, -80° spin phase). One of the major oddities of these spin curves is the lack of broadening of the field-aligned measurements. Indeed, the only difference between the 0 V bias and the -2, -4, and -8 V bias along the field line is the normalization (i.e., density). Modeling of the detector response to a change from 0 to -8 V bias shows that the supersonic flow inferred from the 0 V bias data [Nagai et al., 1984] would produce spin curves which broaden substantially as the effective spacecraft potential varies from +3 to -5 V. This interpretation ignores the likelihood that there may have been an adiabatic decrease in pitch angle width as the ions flow out of the ionospheric source region. Such effects will

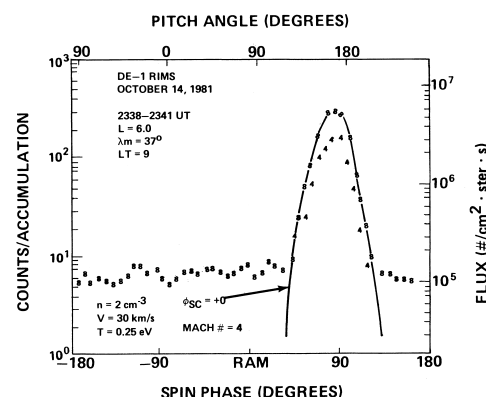


Fig. 11. Hydrogen spin curves for the same period shown in Figure 10.

produce some of the characteristics of these curves, since the pitch angle distributions have widths of 10° - 20° , i.e., less than the detector width ($20^\circ \times 110^\circ$). The ram plasma portion of the spin curve is difficult to model with plasma parameters inferred from the RPA curves unless barrier effects are invoked. It appears that the bulk of the ram plasma is excluded from the detector aperture by a barrier and that the character of the field-aligned flow measurements is determined by a barrier of approximately 4 V. As the bias increases from -4 to -8 V, the barrier height varies only slightly, dropping a few tenths of a volt. This reduces the effect of the 4-V change in detector potential substantially, resulting in spin curves which are nearly unchanged, both for the ram plasma and the field-aligned plasma.

Analysis for the RPA curves taken along the field line turns out to be largely unaffected by the barrier, since the supersonic flow has a bulk energy of 1-2 eV, sufficient to overcome some of the +3 V spacecraft potential at 0 V bias, or the 1 V barrier at -4 or -8 V bias. This interpretation is illustrated by Figure 7, which shows how the energy of the distribution function varies. The major effect is to reduce the flux at 0 V RPA voltage, resulting in a slight underestimate of the ion density. This is illustrated by Figure 8d, RPA curves taken at each aperture bias level, with fits based on the 0 V bias data.

3.1.2. Dayside plasma sheet observations. A slightly different set of ambient plasma conditions is found later on the dayside portion of the orbit, where the ambient plasma density is lower. Plate 2 shows an energy time spectrogram for 3 min of aperture bias data. This time period was shown by Chappell et al. [1982, Plate 2d] and is the first reported observation of the polar wind. These data were analyzed by Sojka et al. [1983].

Previous analysis of these data suggested relatively low Mach numbers, perhaps even subsonic flow. A lack of knowledge of the spacecraft potential was a major problem, which has been resolved in this work by use of the electron data from the HAPI experiment. The result is that the dayside polar wind, measured at $L = 6$, is highly supersonic, with a Mach number of 4-7.

Electron data from the electrostatic analyzer are shown in Plate 2b and Figure 9. Plate 2b is an energy time spectrogram for the same time period as shown in Plate 2a. The locally generated photoelectrons are visible as a yellow band from 5 to 10 eV. The electron distribution function is shown in Figure 9. There is a break, or at least a change in slope, in the distribution function at all pitch angles which separates the locally generated distribution from the ambient population, at the spacecraft potential. (See the appendix for a discussion of this technique.) The break is at 10 eV, suggesting a spacecraft potential of about 10 V. The ambient electron population is characterized by a density of 2 cm^{-3} (assuming a potential of +10 V) and a temperature of 11 eV.

Figure 10 shows two hydrogen RPA curves taken along the field line at -4 and -8 V aperture bias. Using the spacecraft potential inferred from the electron data (+8 to +10 V), a range of possible plasma parameters is obtained as listed in Table 1. The electron data indicate that the ambient plasma density is about 2 cm^{-3} , which is consistent with a +8 to +10 V potential. Additional information can be inferred from the spin phase distribution shown in Figure 11. The lack of

displacement toward the ram direction shows that the field-aligned flow velocity must be high compared to the satellite velocity, i.e., of the order of 10-50 km/s [see Olsen et al., 1985]. This combination of constraints argues for the Mach 5 to Mach 7 solutions. The -8 V bias data, previously thought to indicate a +4 V spacecraft potential, can now be seen to be the result of the large flow energy of the plasma (5 eV). The -4 V bias data are affected by a barrier which is +1 V with respect to the aperture and +5 to +7 V with respect to the ambient plasma. The -8 V data are associated with a 4- to 6-V barrier which is just overcome by the high flow energy of the hydrogen (see Figure 7).

This interpretation is supported by the spin curves, shown in Figure 11. The data can be fitted with models which match the 0.25 eV, 30 km/s interpretation of the RPA curves, if a spacecraft potential near zero is assumed. Again, however, the spin curves do not change shape as the aperture bias is varied, indicating they are dominated by the 5- to 6-V barrier. This interpretation again ignores the likelihood that the spin curve is partly determined by the pitch angle distribution.

4. SUMMARY AND CONCLUSIONS

Aperture bias data taken in the plasmasphere showed that in the thin sheath regime, the detectors behaved as though they were simply shifting in potential. This produced one undesirable side effect, detector saturation. Aperture biases larger than the plasma thermal energy degraded the effective energy resolution of the instrument in this regime. Outside the plasmasphere, with the space-craft potential at small positive values, barrier effects reduced the effectiveness of the bias, particularly in terms of the isotropic background measurements. High Mach number flows were largely undistorted in the ram direction, but spin curve variations are dominated by the barrier height rather than the satellite potential. The interpretation of the dayside polar wind is shown to be highly super-sonic. This change from earlier interpretation is based more on an accurate knowledge of the satellite potential than on barrier effects.

Analysis of the aperture bias data sets shows that the normal positive spacecraft potentials found in the outer plasmasphere and beyond can be partially compensated by means of the aperture bias. This method is limited by the existence of barrier effects and a possible increase in space-craft potential caused by the biasing. This latter effect would not be as severe on a satellite with more conducting surface area, and it remains clear that a conducting surface is imperative for any scientific satellite. The conclusions of Sojka et al. [1983] on requirements for future thermal plasma measurements are reinforced by the analysis shown here. Active potential control is needed for future satellites. This can be accomplished by means of devices such as plasma emitters which set the entire spacecraft to near zero volts potential, alleviating the problem of nonzero potentials and barrier effects [Olsen, 1981]. Electron detectors capable of measuring the 0.5- to 50.0-eV energy range are needed to complement the ion detectors. Such data are particularly necessary in the absence of potential control. It is clearly possible to measure the transport of thermal plasma into the magnetosphere; the challenge is to do the job properly.

APPENDIX

The technique for inferring positive satellite potential uses the uniqueness of particle trajectories reaching the detector at energies below and above the detector potential (energy). Figure 12 illustrates the two classes of trajectories which are allowed for a typical differential analyzer. Trajectories for particles with energies less than the satellite potential must return to the satellite surface, while those at energies above the satellite potential reach the ambient plasma. Unlike ambient plasma distributions, the two distributions do not mix [Montgomery et al., 1973; Olsen, 1982]. This technique also depends on a lack of sensitivity of the detector to EUV generated photoelectrons within the instrument. The HAPI design is nearly immune to such effects, as demonstrated by a near zero (background) count rate when the satellite is in the plasma-sphere, and near zero volts potential.

Alternate explanations of the electron distribution function are possible. Given a photoelectron sheath around the satellite, space charge effects could cause the formation of a potential barrier to electrons leaving the satellite. This would cause the phase space boundary to be at an energy greater (with respect to the satellite) than the satellite potential. The result would be an overestimate of the satellite potential. Extensive thermalization of the local photoelectrons in the sheath would blur the sharp boundary in phase space, with uncertain effects on the potential estimate.

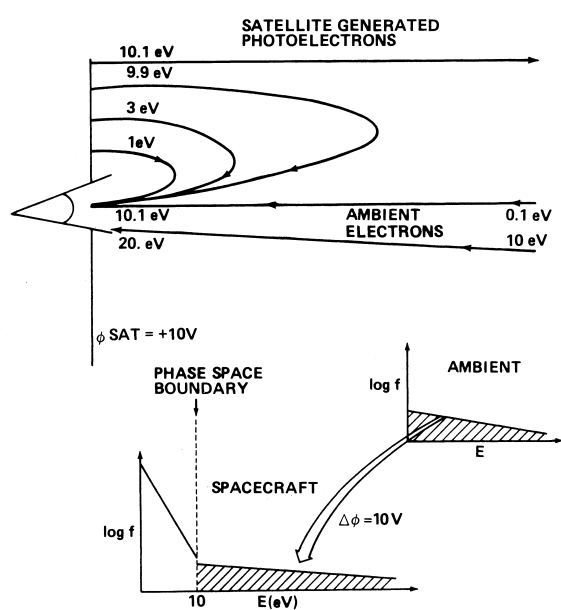


Fig. 12. Electron trajectories and phase space boundaries for a satellite charged to +10 V.

Acknowledgments. The authors would like to express their gratitude to the Data Systems Technology Program and the Space Physics Analysis Network (SPAN) for providing computer and networking facilities. Thanks to J. D. Menietti for processing the HAPI data and to M. Sugiura for use of his magnetic field data in the determination of the particle pitch angles. The research at the University of Alabama in Huntsville was supported by NASA contract NAS8-33982 and NSF grant ATM8-300426. The authors are indebted to the engineering and science staff of the University of Texas at Dallas and to the RIMS team at Marshall Space Flight Center. We are grateful to the programming staff of the Intergraph and Boeing corporations for assistance with the data reduction software.

The Editor thanks E. C. Whipple and another referee for their assistance in evaluating this paper.

REFERENCES

- Burch, J. L., J. D. Winningham, V. A. Blevis, N. Eaker, W. C. Gibson, and R. A. Hoffman, High-altitude plasma instrument for Dynamics Explorer-A, *Space Sci. Instrum.*, 5, 455-463, 1981.
 Chappell, C. R., S. A. Fields, C. R. Baugher, J. H. Hoffman, W. B. Hanson, W. W. Wright, H. D. Hammack, G. R. Carignan, and A. F. Nagy, The retarding ion mass spectrometer on Dynamics Explorer-A, *Space Sci. Instrum.*, 5, 477-491, 1981.
 Chappell, C. R., J. L. Green, J. F. E. Johnson, and J. H. Waite, Jr., Pitch angle variations in magnetospheric thermal plasma-initial observations from Dynamics Explorer-1, *Geophys. Res. Lett.*, 9, 933-936, 1982.
 Comfort, R. H., C. R. Baugher, and C. R. Chappell, Use of the thin sheath approximation for obtaining ion temperatures from the ISEE 1 limited aperture RPA, *J. Geophys. Res.*, 87, 5109-5123, 1982.
 Comfort, R. H., J. H. Waite, Jr., and C. R. Chappell, Thermal ion temperatures from the retarding ion mass spectrometer on DE 1, *J. Geophys. Res.*, 90, 3475-3486, 1985.
 Decreau, P. M. E., J. Etcheto, K. Knott, A. Pedersen, G. L. Wrenn, and D. T. Young, Multi-experiment determination of plasma density and temperature, *Space Sci. Rev.*, 22, 633-645, 1978.
 Farthing, W. H., M. Sugiura, B. G. Ledley, and L. J. Cahill, Magnetic field observations on DE-A and -B, *Space Sci. Instrum.*, 5, 551-560, 1981.
 Gallagher, D. L., J. D. Menietti, J. L. Burch, A. M. Persoon, J. H. Waite, Jr., and C. R. Chappell, Evidence of high densities and ion outflows in the polar cap during the recovery phase, *J. Geophys. Res.*, 91, 3321-3327, 1986.
 Johnson, J. F. E., and G. L. Wrenn, Ion measurements on GEOS using a negatively biased sensor on a positively charged spacecraft, Proceedings of the 17th ESLAB Symposium on Spacecraft/Plasma Interactions and Their Influence on Field and Particle Measurements, Noordwijk, The Netherlands, September 13-16, 1983, *Eur. Space Agency Spec. Publ., ESA SP-198*, 63-68, 1983.
 Montgomery, M. D., J. R. Asbridge, S. J. Bame, and E. W. Hones, Low energy electron measurements and spacecraft potential: VELA 5 and VELA 6, in *Photon and Particle Interactions with Surfaces in Space*, edited by R. J. L. Grard, pp. 247-261, D. Reidel, Hingham, Mass., 1973.
 Nagai, T., J. H. Waite, Jr., J. L. Green, C. R. Chappell, R. C. Olsen, and R. H. Comfort, First measurements of the supersonic polar wind in the polar magnetosphere, *Geophys. Res. Lett.*, 11, 669-672, 1984.
 Olsen, R. C., Modification of spacecraft potentials by plasma emission, *J. Spacecr. Rockets*, 18, 462-469, 1981.
 Olsen, R. C., The hidden ion population of the magnetosphere, *J. Geophys. Res.*, 87, 3481-3488, 1982.

- Olsen, R. C., C. E. McIlwain, and E. C. Whipple, Observations of differential charging effects on ATS 6, *J. Geophys. Res.*, 86, 6809-6819, 1981.
- Olsen, R. C., P. M. E. Decreau, J. F. E. Johnson, G. L. Wrenn, A. Pedersen, and K. Knott, Comparison of thermal plasma observations on SCATHA and GEOS, Proceedings of the 17th ESLAB Symposium on Spacecraft/Plasma Interactions and Their Influence on Field and Particle Measurements, Noordwijk, The Netherlands, September 13-16, 1983, *Eur. Space Agency Spec. Publ. ESA SP-198*, 57-61, 1983.
- Olsen, R. C., C. R. Chappell, D. L. Gallagher, J. L. Green, and D. A. Gurnett, The hidden ion population: Revisited, *J. Geophys. Res.*, 90, 12,121-12,132, 1985.
- Parker, L. W., and E. C. Whipple, Theory of spacecraft sheath structure, potential and velocity effects on ion measurements by traps and mass spectrometers, *J. Geophys. Res.*, 75, 4720-4733, 1970.
- Singh, N., and C. R. Baugher, Sheath effects on current collection by particle detectors with narrow acceptance angles, *Space Sci. Instrum.*, 5, 295-305, 1981.
- Sojka, J. J., R. W. Shunk, J. F. E. Johnson, J. H. Waite, and C. R. Chappell, Characteristics of thermal and suprathermal ions associated with the dayside plasma trough as measured by the Dynamics Explorer retarding ion mass spectrometer, *J. Geophys. Res.*, 88, 7895-7911, 1983.
- Taylor, H. A., H. C. Brinton, and C. R. Smith, Positive ion composition in the magneto-ionosphere obtained from OGÖ-A satellite, *J. Geophys. Res.*, 70, 5769-5781, 1965.
- Whipple, E. C., and L. W. Parker, Theory of an electron trap on a charged spacecraft, *J. Geophys. Res.*, 74, 2962-2971, 1969a.
- Whipple, E. C., and L. W. Parker, Effects of secondary electron emission of electron trap measurements in the magnetosphere and polar wind, *J. Geophys. Res.*, 74, 5763-5774, 1969b.
- Whipple, E. C., J. M. Warnock, and R. H. Winkler, Effects of satellite potential on direct ion density measurements through the plasmapause, *J. Geophys. Res.*, 79, 179-186, 1974.
- Wrenn, G. L., J. J. Sojka, and J. F. E. Johnson, Thermal protons in the morning magnetosphere: Filling and heating near the equatorial plasmapause, *Planet. Space Sci.*, 32, 351-363, 1984.

J. L. Burch, Southwest Research Institute, P.O. Drawer 2851, San Antonio, TX 78284.

C. R. Chappell, Space Science Laboratory, NASA Marshall Space Flight Center, Huntsville, AL 35812.

R. C. Olsen, Physics Department, University of Alabama in Huntsville, Huntsville, AL 35899.

(Received December 26, 1984; revised September 30, 1985; accepted October 24, 1985.)